SEA ICE RADAR ALTIMETER SIGNATURE MODELLING EXPERIMENTS

Rasmus Tonboe [(1)], Søren Andersen [(1)] & Leif Toudal Pedersen [(2)]

(1) Danish Meteorological Institute, Lyngbyvej 100, 2100 Copenhagen Ø, Denmark
(2) Ørsted, Bld. 348, Technical University of Denmark, 2800 Kgs. Lyngby, Denmark

ABSTRACT

Scattering at the large horizontal dielectric contrasts of the snow/sea ice system i.e. the snow and ice surface dominate the altimeter total backscatter coefficient. To investigate the temporal and seasonal altimeter backscatter signature variability a forward model is coupled to a thermodynamic and mass model for the snow and sea-ice temperature profile, accumulation, growth, melt and metamorphosis. The thermodynamic and mass model uses an initial snow and ice profile and meteorological data input. *In situ* data collected during the 2003 CRYOVEX joint Danish-German-ESA campaign and the 2004 GreenIce ice camp are used. Our results show that the snow cover is not only important for the microwave signature of sea ice but also the buoyant balance of ice floes as well as the heat-budget. These considerations are included in the discussion.

1 INTRODUCTION

Radar pulses impinging on sea ice experiences reflections on interfaces between the horizontal dielectric contrasts of the snow/ sea ice system i.e. snow surface, internal layers in the snow and the ice surface. These reflections add to the backscattered signal. The aim here is to give a short overview over the quantitative influence of different micro-physical parameters in sea ice and the snow on top of it and how these link to the nadir looking backscatter signature. The backscatter coefficient of snow-free, level sea ice is primarily a function of ice roughness and surface scattering mechanisms dominate backscatter from the snow/ ice system [1]. Dielectric loss (attenuation) together with volume scattering determine the extinction of the propagating signal within snow and ice layers [2].The backscatter signature of sea ice is therefore a complex function of snow and ice surface roughness, permittivity, layer thickness and scatterer size and distribution. Some of these properties are measured for a limited number of locations in the field or modelled using thermodynamic and mass models with meteorological data input for computing the state of snow/ice properties. We use both observed and modelled properties in the following.

2 METHOD

The investigation is in two parts: 1) a snow/ ice parameter specific sensitivity study of the altimeter signature, and 2) a state specific study of the natural altimeter signature variability using a thermodynamic and mass model for the snow and sea-ice temperature profile, accumulation, growth, melt and metamorphosis.

2.1 Thermodynamic model

Physical snow models are used in important applications on land such as avalanche forecasting [3, 4] and hydrological processes in connection with snowmelt [5]. These one-dimensional mass and energy balance models parameterizes snow temperature, density, thickness, liquid water content, grain size and the snow pack energy balance. Such models for snow on land have also been adapted for energy balance studies on sea ice [6] and coupled to microwave emission models on land [7]. Neither of these models have a parameterisation for surface roughness. Our modelling approach is similar to these above and ensures a realistic description of the snow/ice profile state in connection with meteorological events and general snow metamorphosis [8]. The thermodynamic and mass model is initialised by a sequence of layers (at least one ice layer is needed) and a vertical snow and ice temperature profile. The meteorological conditions drives the freezing or melting of ice, the accumulation or melt of snow, the surface energy balance and the snow metamorphosis and temperature profile. Its output is used as input to the altimeter backscatter forward model.

2.2 Altimeter backscatter forward model

The backscatter model uses the physical snow and ice quantities and structure from the thermodynamic and mass model as input i.e. sequence of layers, density, exponential correlation length, thermometric temperature, volumetric liquid water content and a constant roughness here quantified as the fractional flat-patch-area (F). The exponential correlation length is a measure of scatterer size and distribution, see e.g. [9]. No specific correction is applied for antenna gain or pulse modulation. We use a geometric descrption of the pulse interaction with layers similar to [10, pp. 12-14]. The model is comparable in principle to [11]. In order to apply this model to compute the backscatter it is necessary to

include modules that compute the dielectric properties, and scattering of snow and sea ice. Surface scattering is here synonymous with scattering at horizontal interfaces between layers. Volume scattering is synonymous with scattering from e.g. snow grains within the layers. Surface scattering is computed using the sea ice forward model by [12] where the backscatter coefficient is a function of the fractional area of flat patches (about 3% for sea ice [1]) and the Fresnel reflection coefficient, i.e.

$$\sigma^0 = 0.9FR|0|^2(H/c\tau) \quad \text{(eq. 1)},$$

where F is the fractional flat-patch area, $R|0|$ is the Fresnel reflection coefficient, H the radar height above the surface (800km), c the speed of light in vacuum ($3x10^8$m/s), and τ the pulse length (3.125ns). Small liquid brine inclusions also called brine pockets dominate volume scattering in nilas and first-year ice. In multiyear ice, the voids and air bubbles in the upper ice are the primary scatterers [13]. The permittivity of liquid brine is an order of magnitude larger than the permittivity of solid ice and the permittivity of sea ice is therefore primarily a function of brine volume [14]. The permittivity of brine is computed using appendix E in [14]. The volume scattering in snow and sea ice is computed using the improved Born approximation [15]. The permittivity of snow and sea ice is computed using Polder - Van Santen mixing formulas described in e.g. [16]. It is a function of pure ice permittivity (using [17]), inclusion shape and orientation, volume and the brine pockets permittivity. The formulation in [15] for a media with spherical inclusions is used. Both models above are coded in GNU Octave (www.octave.org).

3 RESULTS & DISCUSSION

During the 2003 CRYOVEX joint Danish-German-ESA campaign two snow and first-year ice micro-physical and temperature profiles were measured in Fram Strait near 76.26ºN, 23.28ºE. The ice thickness in the two profiles is identical (1.5m) while the snow thickness is 7cm and 36cm respectively. The multiyear ice profile is taken as typical for the sea ice around the GreenIce camp in the Lincoln Sea May 2004. Appendix 1 lists the input parameters to the model from the two first-year ice profiles and the multiyear ice profile. Fig. 1 show a situation with snow on sea ice and the terms used in the following.

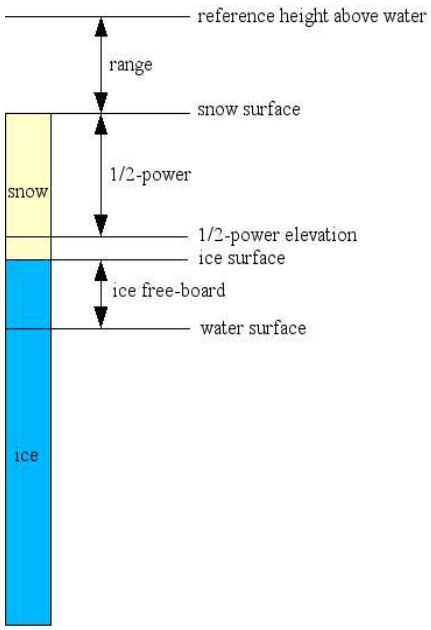

Fig.1. Showing the definition of terms used in the simulations.

Fig. 2b shows the simulated wave-form using the thin and thick snow first-year ice profiles (Fig 2a). The thin snow profile pulse has been delayed by $68x10^{-11}$s which is equivalent to 20cm lower snow surface compared to the thick snow profile for buoyant ice floes. The ice beneath the snow in these two profiles is virtually similar (same thickness and density) and thus fig. 2b shows the significance of the different snow covers for the altimeter wave-form. To investigate the influence of the snow cover on backscatter further the multiyear ice profile is used in a sensitivity study. The model is used to compute the range + ½ – power time (here taken as a measure of elevation) as a function of snow density between 0 and 500kg/m^3 and snow thickness between 0.025 and 0.475m. Only these two snow parameters in the multiyear ice profile are varied in fig. 3 i.e. the ice thickness is constant 3.5m. Fig. 3 show the ½ – power time as a function of the snow cover density and depth. The penetration depth (not shown), the depth where the transmitted unit

power just beneath the surface has decreased to 1/e, in the above simulation (0.3-0.8m) is a function of both snow density and snow thickness. Increasing snow density decrease the snow/ice interface transmission loss and in fact increase penetration depth. The maximum penetration depth is achieved for maximum snow depth and density. The ½ – power time is in particular sensitive to snow depth which decrease the leading edge slope and thereby increase the ½ – power time. It appears from fig. 4 that the snow water equivalent (product of snow density and depth) influences both the ice floe buoyancy and the radar signal thus complicates the assessment of the measured ice free board.

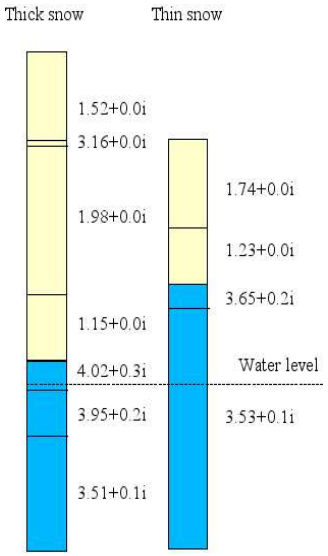

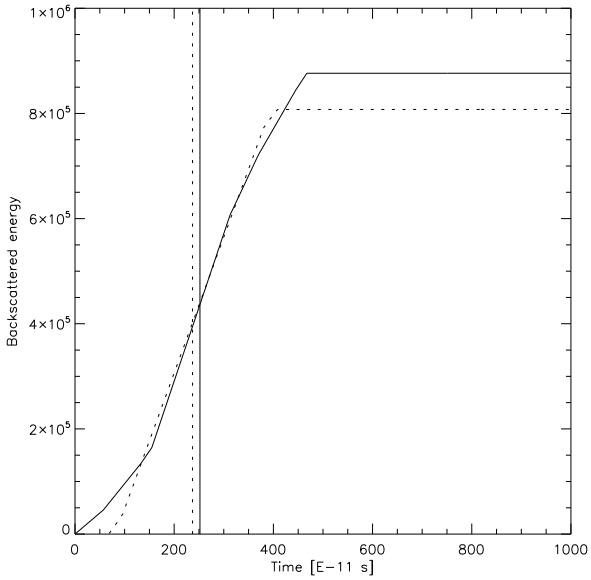

Fig. 2a. (left) The permittivity of the snow and ice layers in the thin and thick first-year ice profiles

Fig.2b. (right) Simulated leading edge of the wave-form for two measured first-year ice profiles with thin 7cm (dotted line) and thick 36cm (solid line) snow cover. The ice thickness in the two cases is the same (1.5m). In buoyant equilibrium, the thick snow surface is 20cm above the thin snow surface. The thin snow profile and its ½ – power time has therefore been delayed by $68x10^{-11}$s (the time it takes light to travel 20cm). The ½ – power time for the thin ($169x10^{-11}$s) and thick ($252x10^{-11}$s) profile is marked with the vertical dashed and solid lines respectively. The thin snow ice surface free-board is 13cm and the thick snow ice surface 4cm. The thin snow penetration depth is 10.5cm and the thick snow profile 40.0cm.

Fig. 5 & 6 show simulated parameters from the thermodynamic and mass and the coupled altimeter backscatter model together with the air temperature. The meteorological record from the GreenIce ice camp in the Lincoln Sea May 2004 used in the thermodynamic and mass model has been modified to investigate the impact of different meteorological conditions. Three precipitation events were added (see fig. 5 text for details). After day 137, 10ºC was added to the air temperature and $20W/m^2$ added to the incoming long-wave radiation to simulate melt. It takes about a day for the multiyear ice profile to adjust to the warmer climate (artificially) imposed on day 137. The upper snow layer starts melting on day 138 and reach liquid water levels around 20% during the day. Even when the liquid water level of the upper snow layer drop to 0% on day 139 the snow pack below continues to be wet throughout the rest of the simulated period. The presence of liquid water in the snow pack has a significant impact on the backscatter parameters. The range + ½ – power time decrease from a level about $400x10^{-11}$s to $300x10^{-11}$s. This reduction in range time is equivalent to about 30cm in free space. The precipitation events increase the penetration depth with about the added snow depth.

Sea ice conditions even within a CRYOSAT resolution cell are often diverse. Large myltiyear ice floes have undulating topography with refrozen melt-ponds and hummocks caused by differential melt in summer, uneven snow cover distribution and pressure ridges. These features all add the backscattered signal and complicates its analysis. However, the melt-pond altimeter backscatter is much higher than backscatter from ridges and hummocks. Therefore, if the model describes backscatter from the melt-ponds adequately it is possible to explain the most important backscatter processes. Our modelling experiments can be seen as an attempt to model multiyear ice melt-pond altimeter backscatter. The snow cover plays a vital role for the melt-pond signature. The snow cover as well as ridges, hummocks, sea ice density etc. are further important for the floe buoyancy, surface energy balance and conductive heat flux from the ocean to the atmosphere.

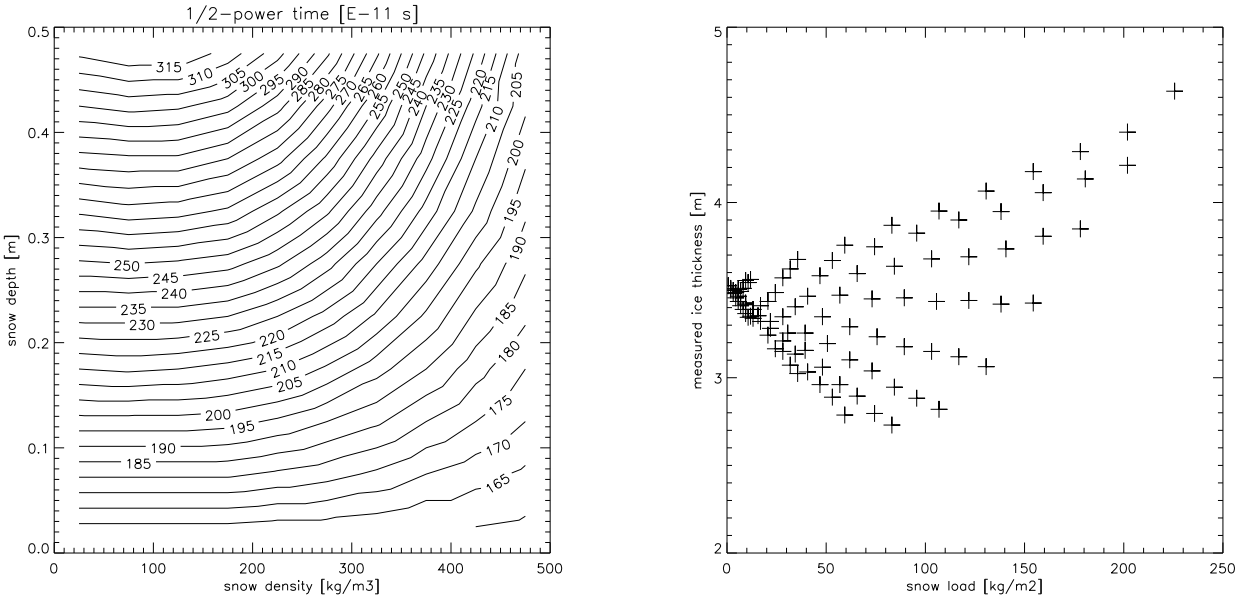

Fig.3. (left) Simulated ½ – power time [1x10^{-11} s] as a function of snow density and snow depth. The snow density and the snow depth of the multiyear ice profile is varied. The radar is at a fixed height above the snow surface. The contour interval time (5x10^{-11}s) is equivalent to 1.5cm in free space.

Fig.4. (right) The snow load [kg/m^2] vs. a simulation of measured ice thickness using ice ½ – power + range time and a water reference for different snow loads (the product of snow density and thickness i.e. the snow water equivalent). In the simulation it is assumed that the ice free board is measured by the ½ – power time + snow surface range to the radar, this range measurement is compared to a 'perfect' (constant) range measurement over water. The free board is then multiplied by 10 to obtain the simulated ice thickness measurement.

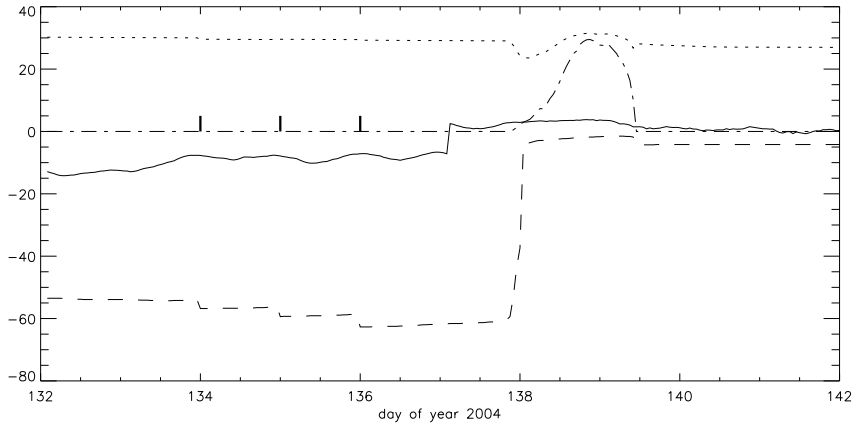

Fig.5. The simulated backscatter coefficient [dB](dotted line), liquid water content of the upper snow layer [%](dash-dotted line) and penetration depth [cm](dashed line) using a modified meteorological record from the GreenIce camp in the Lincoln Sea May 2004 and the multiyear ice profile in Appendix I. The air temperature [ºC] is marked by the solid line and precipitation events on day 134, 135 and 136 of 5kg/m^2 are marked by vertical pins. The original meteorological record had persistent cold (about -10ºC) conditions during the entire 10 day period and both backscatter and snow/ice parameters variability was small. In order to study the effect of different meteorological conditions the three precipitation events were added and 10ºC and 20w/m^2 were added to the air temperature and incoming long-wave radiation respectively after day 137.

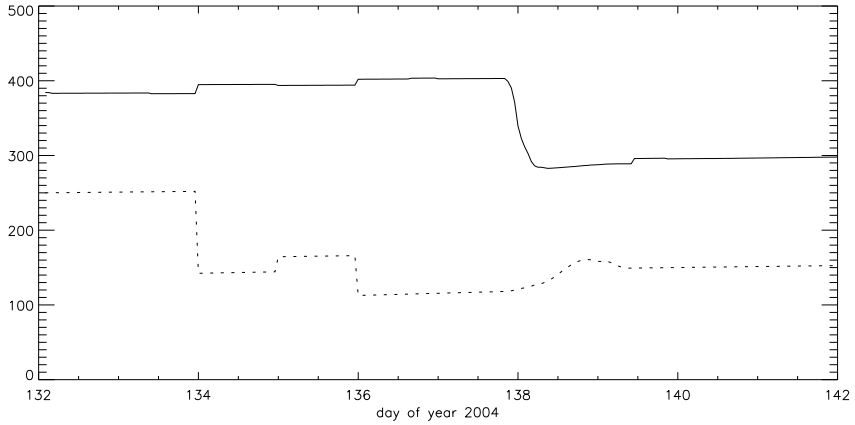

Fig.6. (continued from fig. 5). The range + ½ – power time [$1x10^{-11}$s] (solid line) and the upper snow layer density [kg/m^3] (dotted line) is simulated using a modified meteorological record from the GreenIce camp in the Lincoln Sea May 2004 and the multiyear ice profile in Appendix I.

4 CONCLUSIONS

Different snow cover i.e. snow depth, layering and density has a significant impact on the radar altimeter leading edge.

In particular the snow depth increase the ½ – power time. The snow depth suppress the ice free-board and elevate the snow surface. The simulated buoyant balance and the simulated radar ice elevation measurement counter-balance to some extent (extension of the radar range and elevation of the snow free board). The simulated measurement of ice thickness is accurate within +/- 1m under the different snow conditions.

Backscatter parameters are fairly stable during cold conditions (air temperature < 0ºC). However melt and liquid water in the snow change backscatter parameters dramatically. In our example the range + ½ - power time is reduced by $100x10^{-11}$s at the onset of melt, equivalent to 30cm apparent elevation difference (increase).

Indeed these model experiments indicates that the snow cover and the upper ice characteristics significantly influence the backscatter signature. In order to proceed making sea ice free-board and ice thickness measurements with radar altimeter a description of the snow cover is necessary i.e. snow thickness, density, water content, grain-size. However, reliable hemispheric sea ice snow mapping algorithms using satellite data does not exist today. Future effort to achieve this is urgent if the prophesy of Rothrock should not become reality: '*... to estimate the ice surface* h_t [free-board] *and then multiply by ... 10 to obtain thickness h introduces unsatisfactory errors.*' [18, p. 563].

ACKNOWLEDGEMENTS

This work was supported by the European Commissions 5th framework programme; GreenIce (EVK2-2001-00280). First-year ice profiles in Fram Strait were collected by Christian Haas.

REFERENCES

1. Fetterer, F. M., M. R. Drinkwater, K. C. Jezek, S. W. C. Laxon, R. G. Onstott, & L. M. H. Ulander, Sea ice altimetry. In: F. D. Carsey, Ed.,. *Microwave Remote Sensing of Sea Ice, Geophysical Monograph 68* (pp. 111-135). Washington DC: American Geophysical Union, 1992.
2. Hallikainen, M. & D. P. Winebrenner (1992). The physical basis for sea ice remote sensing. In: F. D. Carsey, Ed., *Microwave Remote Sensing of Sea Ice, Geophysical Monograph 68* (pp. 29-46). Washington DC: American Geophysical Union, 1992.
3. Lehning, M., P. Bartelt, B. Brown, T. Russi, U. Stöckli, & M. Zimmerli, SNOWPACK model calculations for avalanche warning based upon a new network of weather and snow stations. *Cold Regions Science and Technology 30*, 145-157, 1999.
4. Brun, E., E. Martin, V. Simon, C. Gendre, & C. Coleou, An energy and mass model of snow cover suitable for operational avalanche forecasting. *Journal of Glaciology 35*(121), 333-342, 1989.
5. Albert, M.., & G. Krajeski, A fast physically based point snowmelt model for use in distributed applications. *Hydrological Processes 12*, 1809-1824, 1998.

6. Jordan, R. E., E. L. Andreas, & A. P. Makshtas, Heat budget of snow-covered sea ice at North Pole 4. *Journal of Geophysical Research 104*(C4), 7785-7806, 1999.
7. Wiesmann, A., C. Fierz, & C. Mätzler, Simulation of microwave emission from physically modelled snowpacks. *Annals of Glaciology 31*, 397-405, 2000.
8. Tonboe, R. T., A mass and thermodynamic model for sea ice. IOMASA report in preparation.
9. Mätzler, C., Relation between grain-size and correlation length of snow. *Journal of Glaciology 48*(162), 461-466, 2002.
10. Chelton, D. B., J. C. Ries, B. J. Haines, L.-L. Fu, & P. S. Callahan. Satellite altimetry. In: L.-L. Fu & A. Cazenave (Eds.), *Satellite altimetry and Earth sciences*, Academic Press, 2001.
11. Ridley, J. K. & K. C. Partington, A model of satellite radar altimeter return from ice sheets. *International Journal of Remote Sensing 9*(4), 601-624, 1988.
12. Ulander, L. M. H., & A. Carlström, Radar backscatter signatures of Baltic sea ice. *Proceedings of IGARSS'91*, 1215-1218, 1991.
13. Nghiem, S. V., R. Kwok, S. H. Yueh, & M. R. Drinkwater, Polarimetric signatures of sea ice – 1. Theoretical model. *Journal of Geophysical Research 100*(C7), 13665-13679, 1995.
14. Ulaby, F. T., R. K. Moore, & A. K. Fung, *Microwave Remote Sensing, from Theory to Applications, Vol. 3.* Dedham MA: Artech House, 1986.
15. Mätzler, C. Improved Born approximation for scattering of radiation in a granular medium. *Journal of Applied Physics 83(11)*, 6111-6117, 1998.
16. Sihvola, A. H. & J. A. Kong, Effective permittivity of dielectric mixtures. *IEEE Transactions on Geoscience and Remote Sensing 26*(4), 420-429, 1988.
17. Mätzler, C., Microwave properties of ice and snow. In B. Schmitt et al. (Eds.), *Solar System Ices* (pp. 241-257), Kluwer Academic Publishers, 1998.
18. Rothrock, D. A., Ice thickness distribution – measurement and theory. In: N. Untersteiner (Ed.) T*he Geophysics of Sea Ice* (pp. 551-575). NATO ASI series, Series B: Physics Vol. 146. Plenum Press, 1986.

APPENDIX I

The table is showing the ice and snow parameters used as model input parameters. T is the thermometric temperature, F is the fractional flat-patch area, ρ is the density, d is the layer thickness, p_{ec} is the exponential correlation length of scatterers, S is the salinity and i/s indicate whether the layer is snow, s, or sea ice, i.

layer no.	T [°C]	F [%]	ρ [kg/m^3]	d [m]	p_{ec} [mm]	S [psu]	i/s
Thin snow first-year ice profile							
1	-20.15	5.0	400	0.04	0.07	0.00	s
2	-16.55	1.0	150	0.03	0.15	0.00	s
3	-14.15	2.0	920	0.05	0.19	13.5	i
4	-10.00	1.0	920	1.45	0.17	7.00	i
Thick snow first-year ice profile							
1	-22.05	5.0	300	0.14	0.07	0.00	s
2	-11.05	1.0	920	0.002	0.10	0.00	s
3	-11.05	1.0	500	0.16	0.10	0.00	s
4	-8.95	1.0	100	0.06	0.15	0.00	s
5	-8.45	2.0	920	0.05	0.22	13.6	i
6	-7.55	1.0	920	0.10	0.21	11.3	i
7	-10.0	1.0	920	1.35	0.17	7.00	i
Multiyear ice profile							
1	-9.61	3.0	250	0.05	0.10	0.00	s
2	-9.06	0.1	250	0.05	0.10	0.00	s
3	-8.56	0.1	250	0.05	0.10	0.00	s
4	-7.97	0.1	250	0.05	0.10	0.10	s
5	-7.43	0.1	250	0.05	0.25	0.50	s
6	-7.35	3.0	900	0.05	0.35	1.00	i
7	-7.27	0.0	900	0.20	0.35	1.00	i
8	-6.94 ... -1.8	0.0	900	3.30	0.25	2.50	i